RSC Advances

PAPER

View Article Online
View Journal | View Issue

Cite this: *RSC Adv.*, 2019, **9**, 11576

In vivo targeting of breast cancer with a vasculature-specific GQDs/hMSN nanoplatform

Jingjing Dong,†[a] Xinyue Yao,†[ab] Shian Sun,[c] Yuanyuan Zhong,[a] Chuntong Qian[a] and Dongzhi Yang *[ad]

According to our previous experiment, graphene quantum dots capped in hollow mesoporous silica nanoparticles, denoted as GQDs@hMSN, and its conjugates exhibited great potential for medical applications due to their commendable biocompatibility. Due to the fluorescence and structural stability, and enormous porosity, polyethylene glycol (PEG) modified GQDs@hMSN (GQDs@hMSN-PEG) is a good candidate in a drug carrying and delivery system. However, the goal of targeted drug delivery couldn't be achieved simply by utilizing the enhanced permeability and retention (EPR) effect of tumors. In this study, GQDs@hMSN-PEG was further functionalized with vascular endothelial growth factor antibodies (VEGF Abs) for VEGF targeting of breast tumors. Doxorubicin (DOX) was loaded into GQDs@hMSN-VEGF Abs with a drug loading capacity of 0.80 mg DOX per mg GQDs@hMSN. With GQDs as the fluorescent source, GQDs@hMSN-VEGF Abs demonstrated strong fluorescence intensity in VEGF-positive cells. Results from *in vitro* and *in vivo* targeting experiments indicated that GQDs@hMSN-VEGF Abs had high specificity on tumor vasculature, and it could be used as an image-guidable, tumor-selective delivery nanoplatform for breast cancer.

Received 11th March 2019
Accepted 5th April 2019

DOI: 10.1039/c9ra01833f

rsc.li/rsc-advances

Introduction

Low efficiency is a major factor in the failure of nano drug delivery.[1,2] The high permeability and long-lasting effect of solid tumors provide the possibility of tumor-targeted drug delivery of nanomaterials, and the targeting properties of monoclonal antibodies (mAbs) targeting tumor cells are also improved to some extent. However, most of the nanomaterials can't penetrate the blood vessel barrier into the tumor target area only by targeting tumor cells, resulting in inefficient drug delivery of nanomaterials.[3] Tumor angiogenesis plays an important role in tumor growth and metastasis. Compared with cell targeting, vascular-targeted drugs can avoid vascular barriers, and can accumulate rapidly in high concentrations in target sites after administration. Therefore, tumor vascular targeting is a more efficient delivery method for nanomaterials.

In China, the incidence of breast cancer ranks first in female malignant tumors, and 90% of patients die of tumor metastasis.[4,5] Traditional chemotherapy drugs can't effectively distinguish tumor cells and normal cells, cause toxicity and adverse reactions, and are prone to drug resistance. The use of drug-loaded systems minimizes the toxic side effects of the drug, and the optical or radiological properties of certain drug-loaded systems allow for the *in vivo* distribution of the drug and the therapeutic monitoring of the tumor. Based on this, the design and application of a drug-loading system integrating chemotherapy and tracer imaging is expected to solve this problem. VEGF is one of the most important factors regulating angiogenesis and plays an important role in tumor neovascularization. There are four subtypes of VEGF mRNA in human breast cancer tissue: VEGF121, VEGF145, VEGF165 and VEGF189, of which VEGF189 has the highest expression. The content of VEGF in the normal breast duct epithelium is very low, while in breast cancer patients, the VEGF content is significantly increased.[6] Studies have shown that the expression level of VEGF is positively correlated with the size of breast cancer, and high expression can promote distant metastasis of breast cancer.[7]

Graphene is a two-dimensional monolayer sheet-like carbon nanomaterial, which is an important carbon-based nanomaterial because of its large two-dimensional planar structure, high specific surface area, good biocompatibility, and longevity. The performance characteristics of the body's circulation time make it a huge application space for drug carriers. So far, researchers have prepared nanometer-micrometer graphene derivatives.[8,9] Graphene quantum dots (GQDs) is a representative member of the graphene family. It is a small piece of graphite with a size of less than 10 nm. Due to its excellent biocompatibility and good optical performance, fluorescence

[a]*Jiangsu Key Laboratory of New Drug Research and Clinical Pharmacy, Xuzhou Medical University, Xuzhou, Jiangsu 221004, China. E-mail: dongzhiy@xzhmu.edu.cn; Tel: +86-516-63262138*

[b]*Jiangsu Vocational College of Nursing, Huai'an, Jiangsu, 223001, China*

[c]*Xuzhou Air Force College, Xuzhou, Jiangsu 221000, China*

[d]*Department of Pharmaceutical Analysis, Xuzhou Medical University, Xuzhou, Jiangsu 221004, China*

† These authors contributed equally to this work.

properties based on its size are widely used in bioimaging.[10,11] Zhang[12] used GQDs stimulated by yellow light to simultaneously monitor neural stem cells, pancreatic stem cells, and cardiac stem cells. Based on their research, GQDs mainly remains in the cytoplasmic region of stem cells without affecting their normal survival, proliferation, and differentiation. Nurunnabi[13] prepared a series of different color GQDs solutions by adjusting the reaction temperature during the carbon fiber oxidation cleavage process. The GQDs was intravenously injected into nude mice. GQDs can be used as a non-invasive probe for *in vivo* imaging. Due to the strong penetration ability and low absorption rate of near-infrared light in tissue, near-infrared quantum dots have obvious advantages in tumor bioimaging. The GQDs synthesized by Ge[14] from polythiophene (PT2) emitted in the near-infrared region, and released singlet oxygen under laser irradiation. These properties endowed GQDs cancer imaging and treatment in clinical applications.

Studies have shown that nanoparticles smaller than 100 nm have good targeting and *in vivo* scavenged capabilities. For example, single-walled carbon nanotubes with a size of 20 to 80 nm can escape from reticuloendothelial cells and are excreted by gallbladder and kidneys. Single-walled carbon nanotubes with a size of 1 to 2 μm can't be eliminated *in vivo*,[15] in addition, unlike aggregates with a size of 100 nm, particles with a size of 20 to 50 nm can escape from macrophages[16,17] thus facilitating *in vivo* and *in vitro* applications. Nanomaterials need to be purified and sized before they are used in the medical field. Liu's group used gradient centrifugation to separate PEG-functionalized monolayer graphene with a size of about 20 nm.[18] However, because free PEG is easily adsorbed on the surface of graphene, its further biological applications are limited.

High-quality graphene quantum dots can be prepared by hydrothermal method.[19] However, the size of graphene quantum dots is less than 10 nm, and they are easily removed by the kidneys *in vivo*, so it is not suitable for directly being used *in vivo* application as a drug delivery system. Further modification becomes a prerequisite for the application of graphene quantum dots in medical imaging and therapy. Silica materials have been identified as "Generally Recognized as Safe" materials by the Food and Drug Administration (FDA) and have good prospects for clinical applications.[20–22] Because of its non-toxicity, simple chemical modification path, and low synthesis cost, silicon oxide-based nanomaterials are widely used in the biological field.[23–25] Among various silica materials, hollow mesoporous silica nanoparticles (hMSNs) with high biocompatibility are one of the most promising nano drug carriers.[26] Especially with the convenient loading and release of source materials, rich surface charge facilitates the link with biological macromolecules, hMSN has attracted more and more attention, especially in drug delivery system and cancer treatment.[27,28]

In this work, GQDs@hMSN-VEGF Abs nanoplatform was formed with hMSN as the shell, GQDs as the core, DOX as the drug model and VEGF Abs as the recognition reagent. Flow cytometry and confocal fluorescence microscopy experiments were carried out to testify the targeting specificity of GQDs@hMSN-VEGF Abs against VEGF. *In vivo* fluorescence imaging determined their biodistribution. Results from *in vitro* and *in vivo* indicated that the prepared nanoplatform could not only have good biocompatibility, but also target VEGF and specifically release drugs in tumor. From the experimental results, the prepared GQDs@hMSN conjugates can be used as a candidate in image-guided drug delivery and targeted cancer therapy.

Experimental section

Chemicals and reagents

Rabbit polyclonal antibodies to VEGF were got from Abcam. Succinimidyl carboxymethyl PEG maleimide (SCM-PEG-Mal, MW = 5 kDa) was purchased from Yanyi Biological Co. Ltd. (Shanghai, China). PD-10 size exclusion columns were purchased from GE Healthcare. Tris(2-carboxyethyl) phosphine (TCEP) was purchased from Fisher Scientific. Thiophene-3-boronic acid, 3-thiophene-acetic acid, tetrakis(triphenylphosphine) palladium, 4-bromobenzyl bromide, 1-(3-dimethylaminopropyl)-3-ethylcarbodiimide hydrochloride, *N*,*N*-dimethyldodecylamine 6-bromo-1-hexanol, 4-(dimethylamino)pyridine, and 1,4-diazabicyclooctane were purchased from Alfa Aesar. Cetyl trimethylammonium chloride (CTAC) and 3-ammonia propyl trimethoxy silane (APS) were purchased from J & K Technology Co. Ltd. Tetraethyl orthosilicate (TEOS) and triethanolamine (TEA) were purchased from Aladdin. Traut's reagent was got from Fisher Scientific. (*S*)-2-(4-Isothiocyanatobenzyl)-1,4,7-triazacyclononane-1,4,7-triacetic acid (*p*-SCN-Bn-NOTA, abbreviated as NOTA) was purchased from Macrocyclics, Inc. (Dallas, TX, USA). Water was treated by Millipore filtration system.

Synthesis of GQDs@hMSN conjugates

GQDs@hMSN were prepared according to our previous work.[29] Briefly, 4-bromobenzyl bromide (0.25 g) was dissolved in CH_2Cl_2/CH_3OH (20 mL, v/v = 3/2), followed by adding *N*,*N*-dimethyldodecylamine (0.4 mL), allowing the reaction for 12 h at room temperature (RT). After being concentrated to 5 mL, the residue was purified with absolute diethyl ether in triple to form compound 1 as a white solid. 0.4 g compound 1, 0.5 g Na_2CO_3, 200 mg $Pd(PPh_3)_4$ and 0.128 g thiophene-3-boronic acid were mixed into water/ethanol. After refluxing at 90 °C for 6 h by a Suzuki reaction, compound 2 was given. Catalyzed compound 2 by $FeCl_3$, PT2 was synthesized *via* an oxidative polymerization. PT2 dissolved in NaOH solution (0.5 mM) was hydrothermal treated at 160 °C for 24 h followed by ultrasonic treatment. After being centrifuged and filtered against water, GQDs were purified.

With GQDs as the crystal seeds, GQDs@hMSN was prepared according to our previous work.[30] Briefly, GQDs powder was dissolved in absolute ethanol, followed by adding TEOS to form GQDs@dSiO_2. After purifying with water, GQDs@dSiO_2 was added into the mixed solution of CTAC and TEA, followed by dropwise adding TEOS and allowed reacting for 1 h at 80 °C to form GQDs@dSiO_2/SiO_2 NPs. Decreasing the temperature to 50 °C, Na_2CO_3 powder was added to etch GQDs@dSiO_2/SiO_2 NPs, which allowed reacting for 30 min. After purifying with NaCl : methanol (1%) solution, the GQDs@hMSN was achieved. Hydrolyzing APS in absolute ethanol, GQDs@hMSN was modified with amino group on the surface. For further

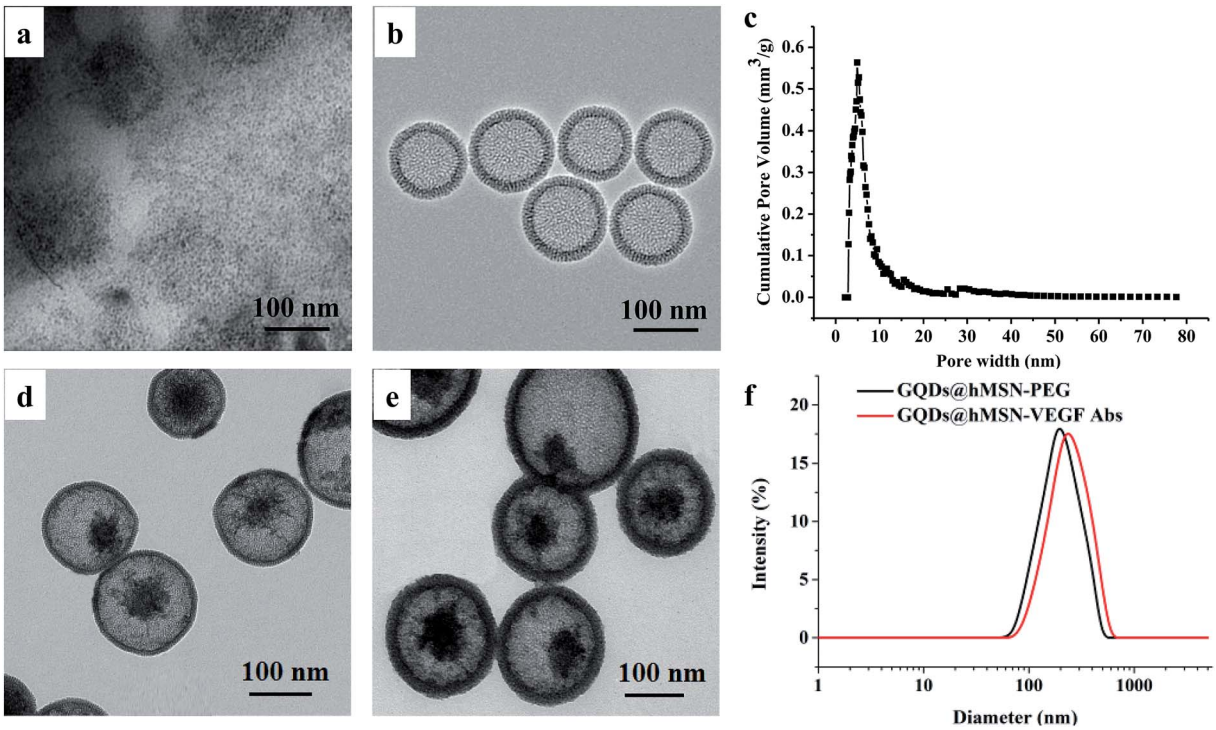

Fig. 1 The structural and morphological characteristics of the prepared GQDs, hMSN and GQDs@hMSN conjugates. (a) TEM image of GQDs; (b) TEM image of hMSN; (c) pore size distribution of hMSN; (d) TEM image of GQDs@hMSN-PEG; (e) TEM image of GQDs@hMSN-VEGF Abs; (f) DLS of GQDs@hMSN-PEG and GQDs@hMSN-VEGF Abs.

functionalization with antibody, SCM-PEG$_{5k}$-Mal was conjugated to GQDs@hMSN based on the reaction between amino and SCM group. Filtering the product with 50 kDa cut off filters, GQDs@hMSN-PEG NPs were gotten.

The attachment of VEGF Abs conjugates was obtained based on the reaction between the thiolated VEGF Abs and MAL group. Briefly, VEGF Abs was thiolated by reacting with Traut's reagent. After being purified by PD-10 column using phosphate-buffered saline (PBS) as the mobile phase, the thiolated VEGF Abs reacted with GQDs@hMSN-PEG overnight at RT under TCEP protecting thiols from being oxidized. The final products termed GQDs@hMSN-VEGF Abs were obtained after being purified by PD-10 elution.

Material characterization

Absorption and fluorescence spectra were recorded in Hitachi U-3010 and F-4600 spectrophotometers, respectively. Transmission electron microscopy (TEM) images were taken on a G2T12 transmission electron microscope (FEI, USA). The hydrodynamic size and surface potentials were determined by dynamic light scattering (DLS) (380 ZLS, NICOMP, USA), at the concentration of 0.05 mg mL^{-1} (based on GQDs@hMSN).

Drug loading/releasing measurement

The drug loading capacity was evaluated by testing the content of doxorubicin (DOX) in GQDs@hMSN conjugates. In brief, GQDs@hMSN-VEGF Abs (~1.5 mg mL^{-1}) was mixed with DOX (1 mg mL^{-1}) at pH 8.0 overnight. The unbound excess DOX was removed by purifying it with PBS thrice. The drug release curves was obtained by determining the concentration of DOX after incubating GQDs@hMSN(DOX)-VEGF Abs in different medium (acetate buffer with pH value of 5.0 and 6.5, phosphate buffer with pH value of 7.4) at 37 °C. The amount of released DOX was calculated according to its absorbance at 485 nm.

Cell line and animal model

MCF-7 and fibroblasts cells L929 were cultured in RPMI 1640 medium containing 10% fetal bovine serum and 1% penicillin/streptomycin with regular cell culturing temperature of 37 °C and 5% CO_2. Cytotoxicity was tested by seeding cells in a 96-well plate, followed by GQDs@hMSN-PEG or GQDs@hMSN-VEGF Abs treatment. Incubating cells in different concentration of GQDs@hMSN-PEG or GQDs@hMSN-VEGF Abs for 24 h, the cells relative viabilities were evaluated by a cell titer 96 kit following vendor's protocols.

All animal procedures were performed in accordance with the National Academy of Sciences Guide for the Care and Use of

Table 1 The ζ-potential of GQDs@hMSN conjugates

Nanoparticles	Zeta potential value (mV)
GQDs@hMSN	11.86 ± 0.3
GQDs@hMSN-PEG	−2.20 ± 0.02
GQDs@hMSN-VEGF Abs	−23.71 ± 0.4

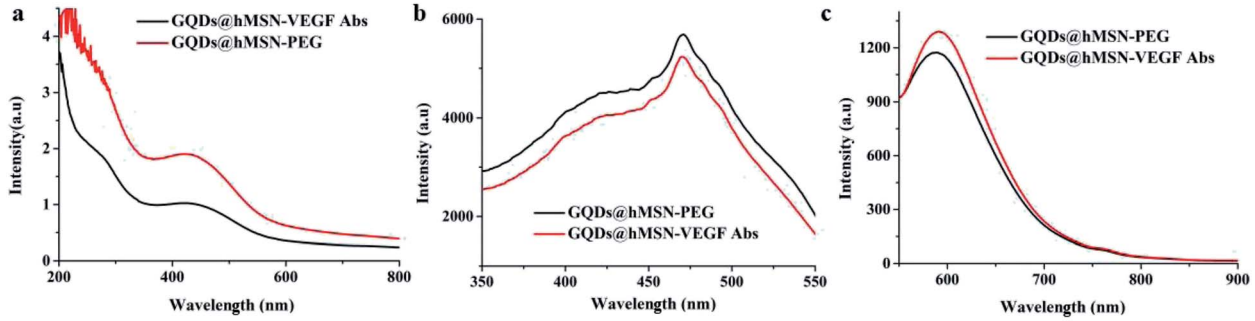

Fig. 2 The optical properties of GQDs@hMSN-PEG and GQDs@hMSN-VEGF Abs. (a) UV-Vis absorbance spectra; (b) excitation spectra; (c) emission spectra.

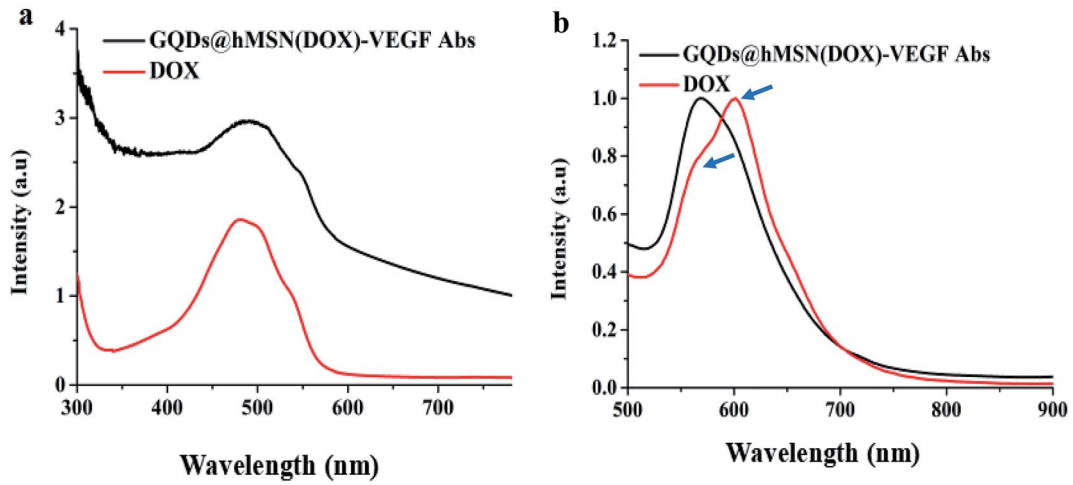

Fig. 3 The optical properties of DOX and GQDs@hMSN(DOX)-VEGF Abs. (a) UV-Vis absorbance spectra, (b) emission spectra.

Laboratory Animals of USA[31] and approved by the Animal Ethics Committee of Xuzhou Medical University. Female BALB/c nude mice (6 weeks, 18–22 g) were used in *in vivo* experiments. 1×10^6 of MCF-7 cells in 50 μL of PBS was subcutaneously injected into the BALB/c nude mice to establish tumors. When the tumor diameter reached 5–8 mm, the mice were used for imaging and drug delivery study.

In vivo drug delivery evaluation

In the *in vivo* drug delivery study, the GQDs@hMSN conjugates including GQDs@hMSN-PEG, GQDs@hMSN-VEGF, GQDs@hMSN(DOX)-PEG and GQDs@hMSN(DOX)-VEGF Abs (5 mg kg^{-1} based on GQDs@hMSN) were separately injected intravenously into MCF-7 tumor-bearing mice. After 2 h, the mice were sacrificed and the main tissues were taken out for *ex vivo* fluorescence imaging (Ex/Em: 485/680 nm) in the Berthold LB983 NightOWL II system.

GQDs@hMSN was mixed with *p*-SCN-Bn-NOTA at a molar ratio of 1 : 10 at pH 9.0 for 1 h. With SCM-PEG_{5k}-Mal as the bridge, the NOTA linked with GQDs@hMSN-VEGF Abs to form NOTA-GQDs@hMSN-VEGF Abs. $^{64}CuCl_2$ (~185 MBq, in 0.1 M HCl) diluted with 0.1 M sodium acetate (pH 6.5) was added to GQDs@hMSN-VEGF Abs. The reaction usually took 1 h at 37 °C with constant shaking. ^{64}Cu-NOTA-GQDs@hMSN-VEGF Abs was purified by a PD-10 column using PBS as the mobile phase. In order to determine the circulation half-life ($t_{1/2}$) of ^{64}Cu-NOTA-

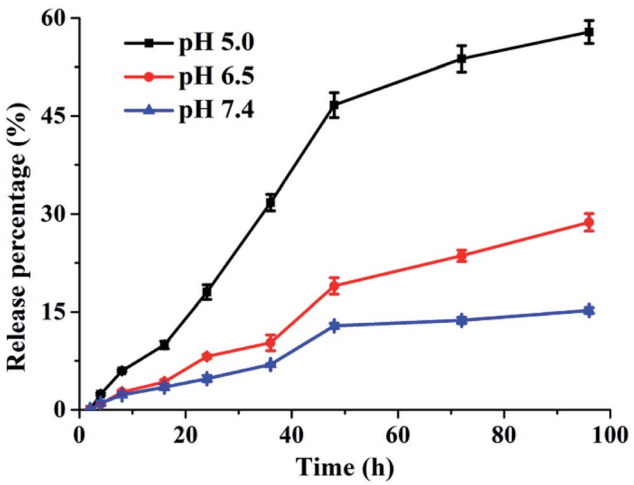

Fig. 4 Drug release of DOX from GQDs@hMSN-VEGF Abs in different medium.

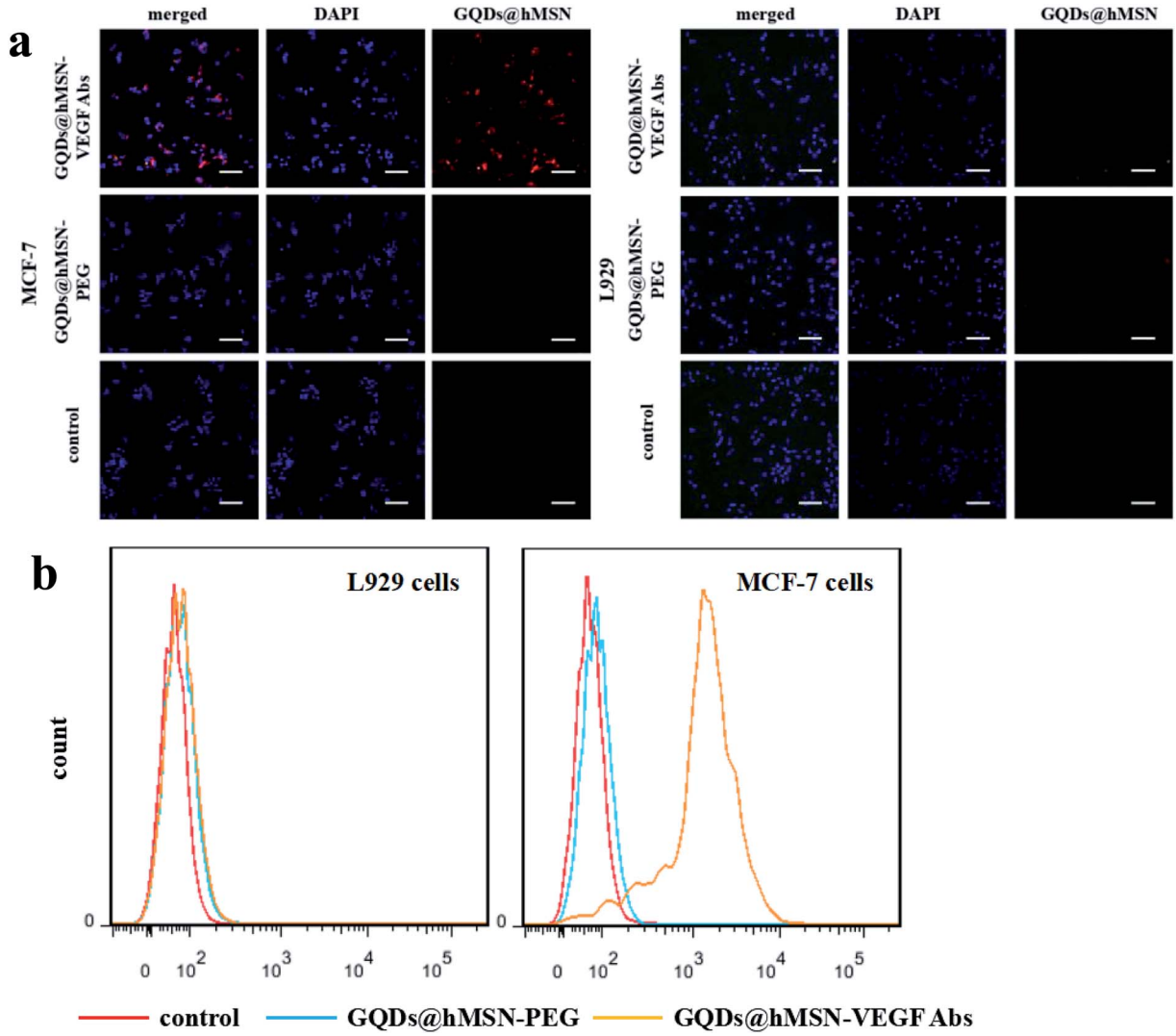

Fig. 5 *In vitro* specificity evaluation of GQDs@hMSN-PEG conjugates. (a) Confocal fluorescence microscopy images of MCF-7 (VEGF+) and L929 cells (VEGF−) incubated with GQDs@hMSN-PEG and GQDs@hMSN-VEGF Abs. Scale bar: 100 μm. (b) Flow cytometry analysis of GQDs@hMSN-PEG and GQDs@hMSN-VEGF Abs in MCF-7 and L929 cells (incubation time: 0.5 h).

GQDs@hMSN-VEGF Abs, mice were subjected to a 30 min dynamic positron emission tomography (PET) acquisition.

Statistical analysis

Data was evaluated with analysis of variance (ANOVA), and differences between groups were analyzed for statistical significance using the Bonferroni *t*-test. $p < 0.05$ was considered to be statistically difference. $p < 0.01$ was considered to be significantly statistical difference.

Results and discussion

Materials characterization

As shown in Fig. 1, the as-synthesized GQDs@hMSN were spherical nanoparticles with the size of 100–150 nm based on TEM measurement. From TEM imaging, the size of GQDs@hMSN aggregates increased slightly after surface linking with VEGF Abs, from *ca.* 120 nm (GQDs@hMSN) to *ca.* 150 nm (GQDs@hMSN-VEGF Abs), which further validated by DLS results. Nanoparticles were easily hydrated in aqueous solution, the size obtained from DLS curve was bigger than that from TEM images. As shown in Table 1, significant change of surface charge was observed after SCM-PEG-Mal coating (ζ-potential: from 11.86 ± 0.3 mV to −2.20 ± 0.02 mV) and after attachment of the VEGF Abs (ζ-potential: from −2.20 ± 0.02 mV to −23.71 ± 0.4 mV).

The optical characteristics were validated by absorption and fluorescence spectroscopy. Fig. 2a showed that both GQDs@hMSN-PEG and GQDs@hMSN-VEGF Abs exhibited broad absorption at the range of 200–500 nm. Both characteristic absorption peaks of GQDs@hMSN-PEG and GQDs@hMSN-VEGF Abs are about 450 nm, which is consistent with that of excitation spectra (Em = 600 nm) in Fig. 2b. As shown in Fig. 2c, Excited by 450 nm, the fluorescence emitted at about 600 nm. Compared with the emission wavelength of GQDs@hMSN-PEG,

the optical properties of GQDs@hMSN-PEG didn't change significantly after linking with VEGF Abs.

DOX loading and release

Fig. 3a showed the UV-Vis absorption spectra of the DOX and GQDs@hMSN(DOX)-VEGF Abs, where the characteristic absorbance at 485 nm indicated that DOX successfully loaded into GQDs@hMSN. It is consistent with that of fluorescence spectra in Fig. 3b, where the emission wavelength of GQDs@hMSN(DOX)-VEGF exhibited two emission peaks (one for DOX at 580 nm, one for GQDs@hMSN at 600 nm). Based on the measurement of unloaded amount of DOX, the loading content of DOX into GQDs@hMSN-VEGF Abs was calculated to be 0.803 mg DOX per g GQDs@hMSN-VEGF Abs. Results indicated that GQDs@hMSN-PEG possessed a very high DOX loading efficiency.

Incubating GQDs@hMSN(DOX)-VEGF Abs in different medium, the DOX release profiles were obtained. As shown in Fig. 4, 15.8% of DOX could be released after 96 h in pH 7.4 medium, which suggested that loaded DOX within GQDs@hMSN-VEGF Abs was relatively stable under physiological condition. In contrast, when the pH value was decreased to 5.0, the amount of released DOX increased to approximately 57.6% after 96 h. The results confirmed that the DOX in GQDs@hMSN-VEGF Abs can be released and the released behavior was pH-dependent.

In vitro tumor cell targeting

Two cell lines including MCF-7 cells (VEGF positive) and L929 fibroblasts (VEGF negative) were used for *in vitro* specificity evaluation of GQDs@hMSN conjugates. As demonstrated in confocal microscopy in Fig. 5a, the fluorescence intensity from GQDs@hMSN-VEGF Abs was substantially stronger than that from GQDs@hMSN-PEG in MCF-7 cells. On the contrary, both GQDs@hMSN-VEGF Abs and GQDs@hMSN-PEG exhibited very minimal nonspecific binding with L929 cells. Through VEGF receptor-mediated endocytosis, GQDs@hMSN conjugates can be transported into MCF-7 cells. The results indicated that the specific recognition on VEGF positive cells. Similar results were got from flow cytometry examination shown in Fig. 5b, where the fluorescence intensity of GQDs@hMSN-VEGF Abs was obviously higher than non-target group in MCF-7 cells, and GQDs@hMSN-VEGF Abs didn't exhibited specificity for L929 cells.

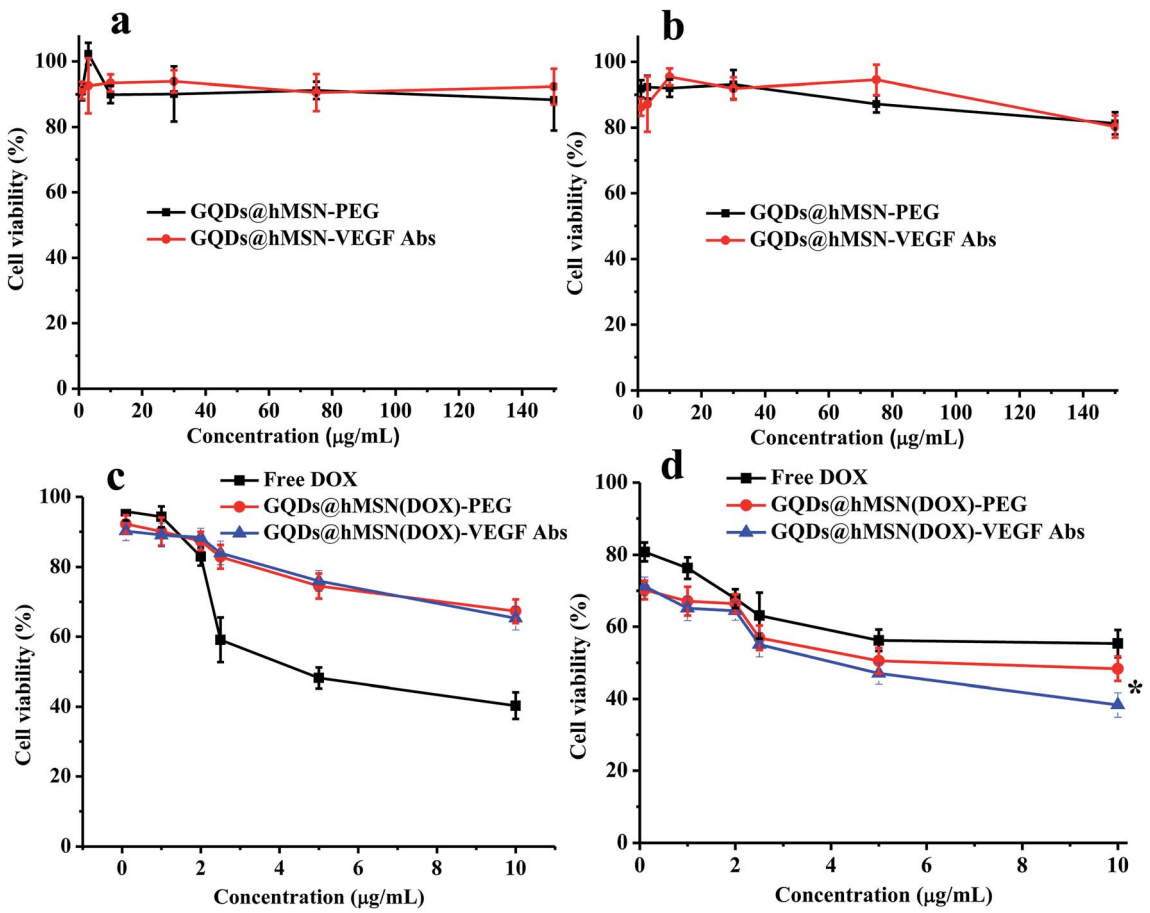

Fig. 6 *In vitro* cytotoxicity of GQDs@hMSN conjugates. (a) *In vitro* cytotoxicity of GQDs@hMSN-PEG and GQDs@hMSN-VEGF Abs in L929 cells; (b) *in vitro* cytotoxicity of GQDs@hMSN-PEG and GQDs@hMSN-VEGF Abs in MCF-7 cells; (c) *in vitro* cytotoxicity of free DOX and released DOX from GQDs@hMSN(DOX)-VEGF Abs and GQDs@hMSN(DOX)-PEG NPs in L929 cells; (d) *in vitro* cytotoxicity of free DOX and released DOX from GQDs@hMSN(DOX)-VEGF Abs and GQDs@hMSN(DOX)-PEG NPs in MCF-7 cells. *$p < 0.05$ *vs.* GQDs@hMSN(DOX)-PEG group.

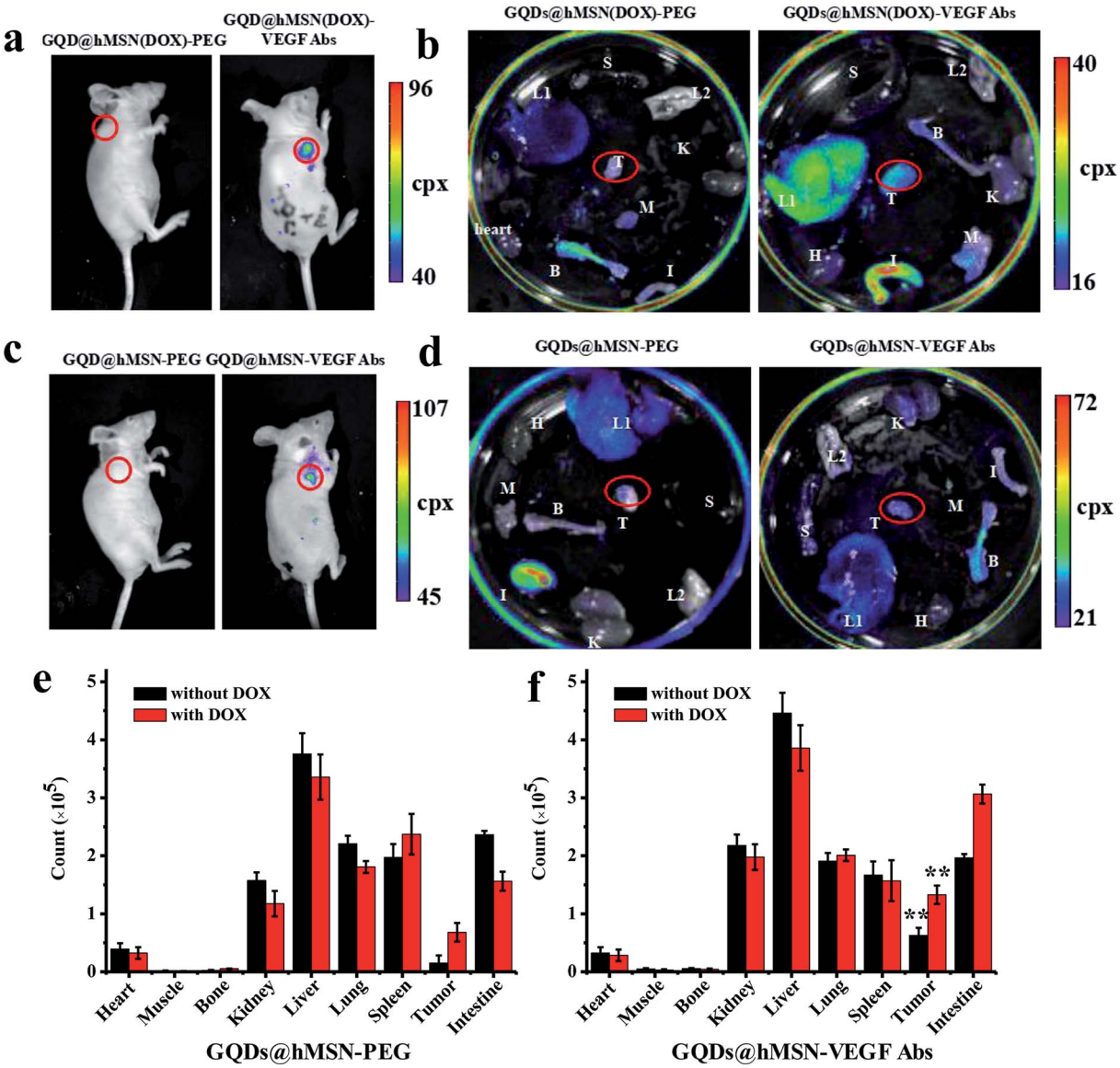

Fig. 7 Serial fluorescence images and *ex vivo* fluorescence signal of mice after intravenous injection of GQDs@hMSN conjugates. (a) Fluorescence images of mice after intravenous injection of GQDs@hMSN(DOX)-PEG or GQDs@hMSN(DOX)-VEGF Abs; (b) *ex vivo* fluorescence images of DOX and GQDs in the major organs/tissues at 30 min after intravenous injection of GQDs@hMSN(DOX)-PEG or GQDs@hMSN(DOX)-VEGF Abs; (c) fluorescence images of mice after intravenous injection of GQDs@hMSN-PEG or GQDs@hMSN-VEGF Abs; (d) *ex vivo* fluorescence images of GQDs in the major organs/tissues at 30 min after intravenous injection of GQDs@hMSN-PEG or GQDs@hMSN-VEGF Abs; (e) *ex vivo* biodistribution in main organs at 2 h post-injection of GQDs@hMSN-PEG; (f) *ex vivo* biodistribution in main organs at 2 h post-injection of GQDs@hMSN-VEGF Abs. T: MCF-7 tumor nodules; L1: liver; L2: lung; K: kidney; H: heart; S: spleen; M: muscle; B: bone; I: intestine. $^{**}p < 0.01$ *vs.* GQDs@hMSN-PEG group.

Safety/toxicity evaluation

Cells viabilities in MCF-7 cells (breast tumor cells) and L929 cells (fibroblasts as the normal control) were carried out to do the cytotoxicity assessment of GQDs@hMSN-VEGF Abs. After incubating with GQDs@hMSN-VEGF Abs for 24 h, over 85% of L929 and MCF-7 cells remain alive showed in Fig. 6a and b. These results revealed that GQDs@hMSN-VEGF Abs exhibited very low toxicity to L929 and MCF-7 cells and had good safety *in vitro*. The cell killing ability of GQDs@hMSN(DOX)-VEGF Abs was also evaluated. Compared with the free DOX, the GQDs@hMSN(DOX)-VEGF Abs exhibited comparable cell toxic effect on MCF-7 cells (in Fig. 6d), which proved the effective DOX release from the nanosystem in tumor microenvironment. From the profile, the lethal concentration (LC50) of GQDs@hMSN(DOX)-VEGF Abs and GQDs@hMSN(DOX)-VEGF Abs was 3.95 and 3.00 μg mL^{-1}, respectively. The cytotoxicity of GQDs@hMSN(DOX) conjugates for L929 cells was lower than that for MCF-7 cells, which maybe attribute to the different release behavior of nanosystem in cells microenvironment.

Organ distribution profile *in vivo*

To investigate the distribution of GQDs@hMSN conjugates in different tissues, we demonstrated the feasibility of drug delivery and imaging *in vivo* using GQDs@hMSN(DOX)-PEG

and GQDs@hMSN(DOX)-VEGF Abs. MCF-7 tumor-bearing mice were injected with GQDs@hMSN-PEG and GQDs@hMSN(DOX)-PEG, as well as GQDs@hMSN-VEGF Abs and GQDs@hMSN(DOX)-VEGF Abs (5.0 mg GQDs@hMSN-PEG per kg, 0.4 mg DOX per kg for both groups). The mice were then sacrificed at 2 h post injection (p.i.), and the major tissues were collected and imaged in the NightOWL II system to detect the tissue presence and biodistribution of GQDs@hMSN-PEG and DOX. From fluorescence imaging observation (Fig. 7), significant fluorescence were found in the tumor with GQDs@hMSN-VEGF Abs, as well as with GQDs@hMSN(DOX)-VEGF Abs. Furthermore, higher fluorescence (about 2-fold of that of GQDs@hMSN-VEGF Abs group) were shown in GQDs@hMSN(DOX)-VEGF Abs group, which emitted both fluorescence of GQDs@hMSN-VEGF Abs and DOX. From time-dependent blood concentrations determination, the half-life ($t_{1/2}$) of GQDs@hMSN-VEGF Abs is relatively long (111.468 min), which allows GQDs@hMSN conjugates to circulate in the blood at a relatively high concentration and continuously extravasate from the blood vessels into the tumor, increasing the VEGF Abs-mediated ligand-receptor binding probability.

Conclusions

By adopting VEGF Abs as a targeting ligand, specific and significantly enhanced targeting of MCF-7 tumor by GQDs@hMSN-PEG conjugates were demonstrated *in vitro* and *in vivo*, which was further confirmed by *ex vivo* organ distribution and histology studies. Furthermore, enhanced DOX delivery to MCF-7 tumors was also demonstrated in tumor-bearing mice. Hopefully this work can encourage other researchers to use different types of GQDs@hMSN nanomaterials for cancer theranostic applications. We are currently trying to further optimize their *in vivo* pharmacokinetics by improving surface engineering methods and investigating the potential of these nanoconjugates for combinational photo dynamic therapy (PDT)/chemotherapy study with GQDs@hMSN-PEG.

Conflicts of interest

There are no conflicts to declare.

Acknowledgements

This work is supported, in part, by the University of Michigan Department of Radiology (startup to H. H.), Natural Science Foundation of Jiangsu Province in China (BK20161173), Postgraduate Research & Practice Innovation Program of Jiangsu Province in China (KYCX18_2200) and Xuzhou Natural Science Foundation in China (KC18201 and KC18108).

References

1 J. Ren, Z. Fang, L. Yao, F. Z. Dahmani, L. Yin, J. Zhou and J. Yao, *Int. J. Pharm.*, 2015, **487**, 177–186.
2 S. R. K. Meka, V. Agarwal and K. Chatterjee, *Mater. Sci. Eng., C*, 2019, **94**, 565–579.
3 Y. Zhang, W. Zhu, H. Zhang, J. Han, L. Zhang, Q. Lin and F. Ai, *Int. J. Pharm.*, 2017, **532**, 384–392.
4 O. J. Scully, B. H. Bay, G. Yip and Y. Yu, *Cancer Genomics Proteomics*, 2012, **9**, 311–320.
5 S. Ghosh, C. A. Sullivan, M. P. Zerkowski, A. M. Molinaro, D. L. Rimm, R. L. Camp and G. G. Chung, *Hum. Pathol.*, 2008, **39**, 1835–1843.
6 M. Toi, H. Bando, T. Ogawa, M. Muta, C. Hornig and H. A. Weich, *Int. J. Cancer*, 2002, **98**, 14–18.
7 H. Hao, Z. Yin, J. Sun and W. Cai, *Nano Today*, 2009, **4**, 399–413.
8 O. C. Compton and S. T. Nguyen, *Small*, 2010, **6**, 711–723.
9 W. M. Deen, *J. Clin. Invest.*, 2004, **114**, 1412–1414.
10 L. Tang, R. Ji, X. Li, K. Teng and S. Lau, *J. Mater. Chem. C*, 2013, **1**, 4908–4915.
11 X. T. Zheng, A. Than, A. Ananthanaraya, D. H. Kim and P. Chen, *ACS Nano*, 2013, **7**, 6278–6286.
12 M. Zhang, L. Bai, W. Shang, W. Xie, H. Ma, Y. Fu, D. Fang, H. Sun, L. Fan, M. Han, C. Liu and S. Yang, *J. Mater. Chem.*, 2012, **22**, 7461–7467.
13 M. Nurunnabi, Z. Khatun, G. R. Reeck, D. Y. Lee and Y. K. Lee, *Chem. Commun.*, 2013, **49**, 5079–5081.
14 J. Ge, M. Lan, B. Zhou, W. Liu, L. Guo, H. Wang, Q. Jia, G. Niu, X. Huang, H. Zhou, X. Meng, P. Wang, C. S. Lee, W. Zhang and X. Han, *Nat. Commun.*, 2014, **5**, 4596.
15 J. Kolosnjajtabi, K. B. Hartman, S. Boudjemaa, J. S. Ananta, G. Morgant, H. Szwarc, L. J. Wilson and F. Moussa, *ACS Nano*, 2010, **4**, 1481–1492.
16 M. Zhang, X. Zhou, S. Iijima and M. Yudasaka, *Small*, 2012, **8**, 2524–2531.
17 M. Zhang, T. Yamaguchi, S. Iijima and M. Yudasaka, *Nanomedicine*, 2013, **9**, 657–664.
18 K. Yang, S. Zhang, G. Zhang, X. Sun, S. T. Lee and Z. Liu, *Nano Lett.*, 2010, **10**, 3318–3323.
19 C. Li and Y. Yue, *Nanotechnology*, 2014, **25**, 435703.
20 S. R. K. Meka, S. K. Verma, V. Agarwal and K. Chatterjee, *ChemistrySelect*, 2018, **3**, 3762–3773.
21 S. Ullah, K. Seidel, S. Türkkan, D. P. Warwas, T. Dubich, M. Rohde, H. Hauser, P. Behrens, A. Kirschning, M. Köster and D. Wirth, *J. Controlled Release*, 2019, **294**, 327–336.
22 M. Li, Y. H. Lao, R. L. Mintz, Z. Chen, D. Shao, H. Hu, H. X. Wang, Y. Tao and K. W. Leong, *Nanoscale*, 2019, **11**, 2631–2636.
23 Z. Li, J. C. Barnes, A. Bosoy, J. F. Stoddart and J. I. Zink, *Chem. Soc. Rev.*, 2012, **41**, 2590–2605.
24 J. Lu, M. Liong, J. I. Zink and F. Tamanoi, *Small*, 2007, **3**, 1341–1346.
25 I. I. Slowing, B. G. Trewyn and V. S. Lin, *J. Am. Chem. Soc.*, 2007, **129**, 8845–8849.
26 X. Yao, Z. Tian, J. Liu, Y. Zhu and N. Hanagata, *Langmuir*, 2017, **33**, 591–599.
27 T. Xia, M. Kovochich, M. Liong, H. Meng, S. Kabehie, S. George, J. I. Zink and A. E. Nel, *ACS Nano*, 2009, **3**, 3273–3286.

28 F. Chen, H. Hong, Y. Zhang, H. F. Valdovinos, S. Shi, G. S. Kwon, C. P. Theuer, T. E. Barnhart and W. Cai, *ACS Nano*, 2013, **7**, 9027–9039.
29 D. Yang, X. Yao, J. Dong, N. Wang, Y. Du, S. Sun, L. Gao, Y. Zhong, C. Qian and H. Hong, *Bioconjugate Chem.*, 2018, **29**, 2776–2785.
30 F. Chen, H. Hong, S. Shi, S. Goel, H. F. Valdovinos, R. Hernandez, C. P. Theuer, T. E. Barnhart and W. Cai, *Sci. Rep.*, 2014, **4**, 5080.
31 National Research Council, *Guide for the Care and Use of Laboratory Animals*, The National Academies Press, Washington, DC, 8th edn, 2011.